Available online at www.sciencedirect.com
ScienceDirect
Aerosol Science 39 (2008) 287–304
Journal of Aerosol Science
www.elsevier.com/locate/jaerosci

Development and experimental evaluation of aerodynamic lens as an aerosol inlet of single particle mass spectrometry

Kwang-Sung Lee, Sung-Woo Cho, Donggeun Lee*

School of Mechanical Engineering, Pusan National University, Busan 609-735, Republic of Korea

Received 13 July 2007; received in revised form 12 October 2007; accepted 29 October 2007

Abstract

This study described a development and an experimental evaluation of an efficient aerodynamic lens inlet of the single particle mass spectrometry. Several key designing parameters and systematic factors were investigated for the whole lens system through a full numerical simulation. From many tests for various designs of the system, we showed that Mach number was not an independent parameter but interrelated well with flow Reynolds numbers and pressures upstream of the orifices. By manipulating the parameters, we showed for the first time a possibility that there exist a universal correlation between optimal Stokes number and a new factor incorporating the other dimensionless variables and a design parameter. The universality was confirmed by the full simulation results. We demonstrated that the new design of the system was capable of focusing ultrafine aerosols in the size range of 30–700 nm. At two different operating conditions, the formations of sub-millimeter beams of 30–300 nm NaCl aerosols are verified by light scattering imaging as well as microprobe observation of deposited aerosol beams. Finally, the measured sizes of aerosol beams agree reasonably well with those from the simulations as a function of particle size.

Keywords: Aerodynamic lens; Aerosol beam; Visualization; Numerical simulation

1. Introduction

Single particle mass spectrometry (SPMS), which is capable of sizing and chemically analyzing single nanoparticle (Carson, Johnston, & Wexler, 1997; Lee, Park, & Zachariah, 2005; Noble & Prather, 2000; Reents & Ge, 2000) has offered an opportunity for better understanding of the controlled syntheses of novel nanoparticles (Mahadevan, Lee, Sakurai, & Zachariah, 2002; Park, Lee, Rai, Mckherjee, & Zachariah, 2005) as well as origin and characteristics of environmental aerosol nanoparticles (Lee, Miller, Kittelson, & Zachariah, 2006). Lee et al. (2006) showed that most of metal-containing particles emitted from a diesel engine lie in the size range of 30–300 nm. Also, such ultrafine and accumulation-mode aerosols can penetrate deeply into human lung and cause serious diseases (Venkataraman & Raymond, 1998). In respect of this aerosol-related health effect, the needs of the advanced SPMS are rapidly growing.

The SPMS consists of an aerodynamic lens (ADL) inlet of aerosols, an assembly of an ion optics and a time-of-flight tube containing an ion detector, a high-power laser as an ionization source and a signal acquisition system. More details about the instrumentation are available elsewhere (Lee et al., 2005, 2006; Mahadevan et al., 2002; Park et al., 2005).

* Corresponding author. Tel.: +82 51 510 2365; fax: +82 51 512 5236.
E-mail address: donglee@pusan.ac.kr (D. Lee).

0021-8502/$ - see front matter © 2007 Elsevier Ltd. All rights reserved.
doi:10.1016/j.jaerosci.2007.10.011

There are two factors determining the performance of the SPMS. The first one would be a hitting rate, i.e., how many particles are detected per second. It is directly proportional to particle concentration existing in the ionization region (laser focus), so that the capability of the ADL inlet to focus aerosols with high transmission determines the hitting rate of the SPMS. The other factor is a quantitative chemical analysis for individual nanoparticle. Recently, we not only raised some issues related to complete ionization, particle size-dependent ion loss and the quantification of the mass spectra (Lee et al., 2005) but also developed a new ion optics capable of resolving the problem (Cho & Lee, 2007). This article is therefore focused on the development and evaluation of the ADL inlet with the purposes of enhancing the hitting rate and thereby applying the SPMS to environmental aerosols at low concentration.

Though sonic or supersonic nozzles with a variety of configurations have been used to produce aerosol beam (Cheng & Dahneke, 1979; Dahneke & Cheng, 1979; Israel & Friedlander, 1967; Murphy & Sears, 1964), the majority of current aerosol focusing systems are the type of aerodynamic lens which is similar in design to Liu, Ziemann, Kittelson, and McMurry's (1995a, 1995b) system. This is because the aerodynamic lens consisting of three-to-five successive orifices produces a narrower beam with higher transmission efficiency for the aerosol particles in a wider size range.

Huffman et al. (2005) summarized well the characteristics and performances of almost all previous ADL systems. Note that their summary was made only on experimental evaluation. Let us briefly address to what extent aerosols could be focused and how they measured the diameters. Liu et al. (1995b) measured aerosol beam diameters downstream of the ADL exit with "knife edge method". Fig 12 in their paper indicated that DMA size-selected NaCl aerosols in the range of 40–200 nm were focused insufficiently into almost 5 mm or larger in diameter. Later then, the same group modified the original design to focus stratospheric aerosols in the size range of 190–1150 nm (Schreiner, Schild, Voigt, & Mauersberger, 1999). But, the resultant beam diameter of NaCl aerosols was larger than 2 mm in diameter. Jayne et al. (2000), who performed a preliminary theoretical study to Zhang et al.'s design (2002, 2004), employed "beam probe method" to measure the aerosol beam diameter. They presented that two types of aerosols with 350 nm of diameter were focused into the narrowest beam. But for smaller sized aerosols, there was no experimental report. Kane and Johnston (2000) reported that the beam diameter of oleic acid aerosols decreased from 0.9 to 0.2 mm as particle size increased from 80 to 200 nm. However, their results were obtained by indirect prediction from measurements of the particle hitting rate of the SPMS. Prather group reported that their ADL system could focus four different sized PSL aerosols (100–290 nm) up to approx. 0.6 mm in full width (Su, Sipin, Furutani, & Prather, 2004). But the beam width was indirectly obtained from the profile of the hit rate of the SPMS. Slowik et al. (2004) measured the beam diameter only for 350 nm flame aerosols by using the beam probe method. Using the same method, Katrib et al. (2005) reported that the various aerosol beam profiles were sharpened to approximately 1 mm in full width. But the measured particles were still as large as 100 nm in diameter. Huffman et al. (2005) proposed a simple model for better design of the beam probe and reported that 100–550 nm volatile aerosols could be focused into a few sub-millimeters to 1 mm. More recently, Wang and McMurry (2006a) developed their own design to focus nuclei-model aerosols smaller than 30 nm. Their aerosol beam size was, however, as large as a few millimeters (2–6 mm for the helium of carrier gas), which seems to be insufficiently focused. Since an ionization laser is readily focused up to hundreds of micrometers (Mahadevan et al., 2002), the laser can miss most of the aerosols in the operation of the SPMS.

As such many researchers seem to follow Liu et al.'s design with no doubt and not to make further theoretical approach to improve or even characterize the design. Recalling the purpose of this study, Liu et al.'s (1995b) system is the only one that was experimentally verified to focus 30–250 nm aerosols to a few millimeters in beam diameter. Now let us turn the attention to theoretical development of the ADL. Since Liu et al.'s (1995a) discovery, only two groups such as Zhang et al. (2002, 2004) and Wang, Kruis, and McMury (2005); Wang, Gidwani, Girshick, and McMurry (2005), and Wang and McMurry (2006b) have devoted to understand particle behavior with numerical simulation, thereby providing their own designs. Zhang et al. (2002) investigated the influences of design parameters such as outer diameter (OD), inner diameter (d_f) and thickness (L) of an orifice, a particle-laden gas flow rate (Q), and upstream pressure (P_{up}) on the performance of the single lens. They extended the single lens study to the design of multi-lens system (Zhang et al., 2004); however, particles smaller than 80 nm were rapidly diverged right after the ADL exit. They successfully find out three dimensionless parameters (Stokes number (St), Reynolds number (Re) and d_f/OD) that play the most important role in particle behavior. However, they failed to provide a certain guideline for the practical design.

Hence, there remains only Wang et al.'s work. Their APL system was theoretically developed to focus 3–30 nm particles in He, rather than to focus 30–300 nm particles in air. They offered a simple guideline for the design. Developing the guideline, Wang and McMurry (2006b) could provide a great design tool that enables to give an optimal design

for any purpose. They certainly made a big step toward not only the synthesis of smaller nanomaterials using the ADL (Fonzo et al., 2000) but also the optimal design of the ADL system. However, their tool is still based on several assumptions or approximations. One of the most critical points is the lack of the knowledge of a functional relationship between the optimal Stokes number and other parameters. Without this, the optimal sizes of each orifice cannot be correctly determined. This might explain why their tool gave much different predictions from the experiments in some region.

Again we would say that it is very rare to find a report that covers both theoretical and experimental evaluation of the ADL in the size range of 30–300 nm. This motivates the present study. From single-lens analysis, we address how key designing parameters work for focusing particles. We then extract optimum sizes of each orifice installed in series. Such a numerical analysis is extended to the whole ADL system. At each orifice while it is assembled, all necessary parameters including the optimal Stokes numbers (St_0) are determined from the full numerical simulation. The required sizes of each orifice are then updated from the values of St_0. In this way, we develop our own design working well for focusing 30–300 nm aerosols. We combine Wang et al.'s guideline with Zhang et al.'s suggestion of the function relations. Eventually, we discover the universal correlation that has been a big challenge for the optimal design. Next, we attempt to evaluate experimentally the focusing capability of the ADL inlet which was assembled to the SPMS. The formation of sub-millimeter beams for 30–300 nm NaCl aerosols in air is verified by light scattering imaging as well as microprobe observation of deposited aerosol beams. Finally, the measured sizes of aerosol beams are compared with those from the simulations as a function of particle size.

2. Experiment

Fig. 1 shows a schematic diagram of the experimental setup to evaluate the ADL inlet of the SPMS. The ADL inlet consists of a flow limiting orifice, five thin orifices (lenses) with various spacers and a flow accelerating nozzle (Lee et al., 2005, 2006; Mahadevan et al., 2002; Park et al., 2005). Fig. 2 shows the magnified drawing of the present ADL excluding the flow limiting orifice. The heart of this design is the easy disintegration of the parts from the ADL system. The spacer separating successive orifices are machined and polished well enough to fit the orifices in the stainless steel

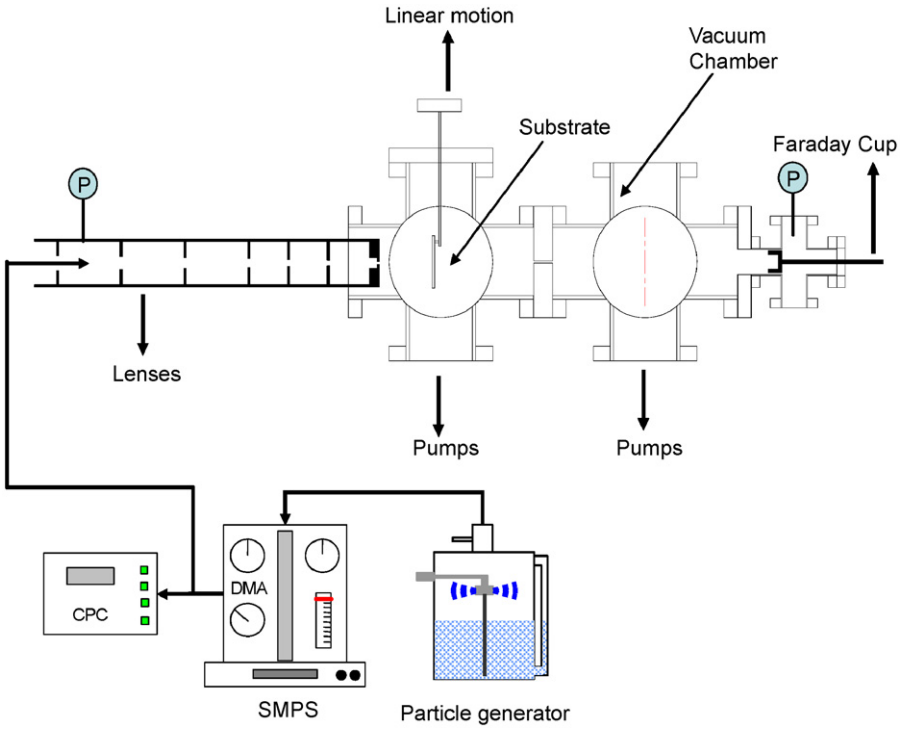

Fig. 1. Experimental setup to evaluate the aerodynamic lens inlet of the single particle mass spectrometry.

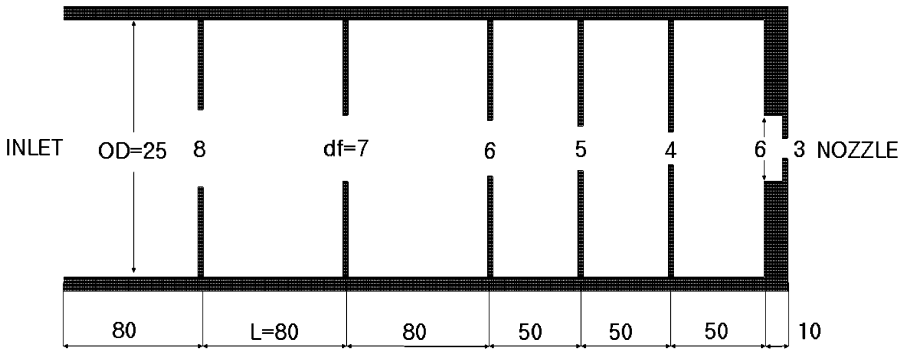

Fig. 2. Schematic of an aerodynamic lens designed to focus 30–300 nm aerosols. The geometric dimensions are in mm.

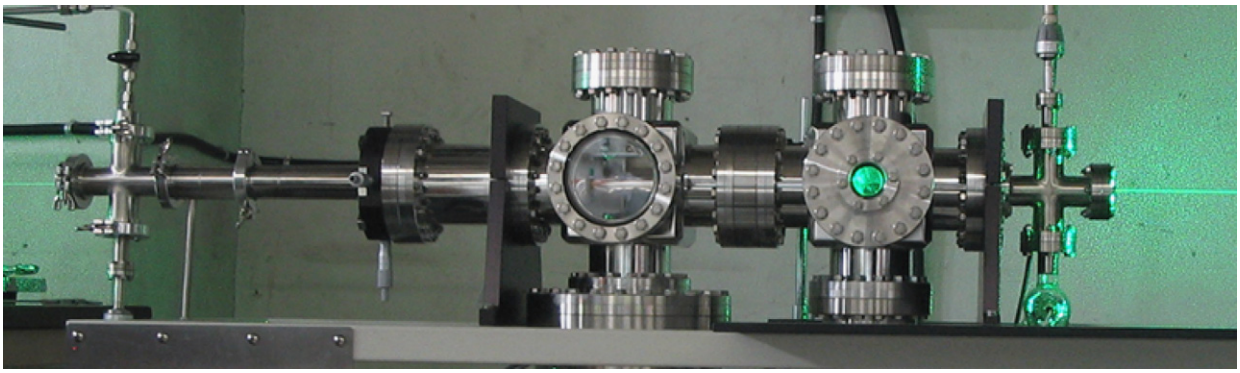

Fig. 3. Photograph for visualization of aerosol beam using light scattering.

housing. Each contacting faces are all vacuum greased to ensure that there is no gas flow through. The flow limiting orifice ($\sim$ 0.1 mm in diameter) fixes the mass flow rate throughout the system at $\sim 2.02 \times 10^{-6}$ kg/s. Therefore, the upstream pressure inside the lens system (right after the flow limiting orifice) is lowered up to $\sim$ 2 torr. The pressure of the first chamber in which the ADL nozzle is located was maintained at $\sim 10^{-2}$ torr by a 1000 L/s turbo pump, whereas the pressure of the second chamber was at 8×10^{-6} torr by a 250 L/s turbo pump, when particle-laden gas flows in. Particles in the size range of 20–300 nm are generated by spraying and drying 1% NaCl–water droplets and details of the generations are available elsewhere (Lee et al., 2005). While air, the most common carrier gas, contracts and expands through an orifice, aerosol particles do not follow the gas stream line but get closer to the centerline of the system due to their higher inertia. Therefore, particles are progressively focused to form a tightly collimated aerosol beam during passing through a series of the orifices. This has been thought as a working principle of the ADL.

Two approaches are used to verify the aerosol collimation in this study. We first attempt to visualize the aerosol beam by light scattering. Fig. 3 shows a photograph of the instrument used in the experiment. A green Ar ion laser beam (Continuum co.) with a continuous power of 0.5 W is aligned exactly counter-propagating to the particle beam through the whole system. For this imaging, the laser beam is slightly defocused with a 1-m long focal length lens so as to encompass the entire particle beam with a sufficient intensity. An air-cooled CCD camera is mounted on the back side of the second chamber. An object lens installed in front of the CCD is used to magnify the image scattered at the center of the chamber. The distance between the exit of the ADL and the center is approximately 210 mm. As a Nd:YAG laser beam is focused at the center to ionize single particle for the chemical analysis, this experiment is designed to visualize the particle beam at the ionization region.

Secondly, we directly deposit the collimated beam of aerosols with different sizes onto a substrate and then observe the deposited layer with an optical microprobe. To facilitate the particle deposition, the Al substrate is vacuum greased. The substrate moves up and down precisely with a precision linear motion feedthrough, that is, mounted 40 mm downstream

of the ADL exit. The deposition experiment of DMA-size selected aerosols has been made for about 90 min. Then the same experiment is repeated for other-sized aerosols.

3. Numerical simulation

A numerical simulation is performed to track particle behavior by utilizing FLUENT (version 6.2.16). Under typical operating condition of the ADL inlet for the SPMS, particle concentration is so low that inter-particle interaction is negligible and the existence of particles hardly affects the gas flow (Wang, Gidwani et al., 2005; Wang, Kruis et al., 2005; Zhang et al., 2002, 2004). Therefore, particle-free gas flow is first calculated under the assumption of axisymmetric, steady, compressible, laminar and viscous flow.

Fig. 4 shows variations of pressure and streamwise velocity of carrier gas along the centerline of the multi-lens system. The pressure decreases in a stepwise fashion and the sudden decrease occurs at each neck of orifice. The flow is obviously subsonic inside the whole ADL system, excluding the downstream of the nozzle exit. But in the nozzle, the pressure is too low to influence particle motion. Wang and McMurry (2006b) suggested that when $Re > 200$, flow instability and turbulence can broaden the particle beam significantly. In the present design, the highest Re (mostly at the nozzle) is always below 100.

Wang and McMurry (2006b) also recommended the use of sufficiently long spacer separating two successive orifices. Gas flow separates from the first orifice aperture and a recirculation zone forms downstream of the orifice as a form of standing vortex as long as the flow is stable and laminar. After a certain distance (reattachment length), the gas flow reattaches to the wall and is then fully developed within a distance from the first orifice (redevelopment length). The two characteristic lengths increase with the Re. If the length of the vortex is comparable to that of the spacer, the successive orifices mutually interact. Fig. 5 confirms all spacers are long enough for the flow to be stable and fully developed.

If the flow Knudsen number (Kn) is smaller than 0.1, the flow is assured in the regime of continuum (Wang & McMurry, 2006b). The Kn was defined as the ratio of mean free path of carrier gas to the radius of the orifice aperture. In our case, the highest Kn at the nozzle is ca. 0.012, so that the flow is safe in the regime. Then particles with a specified diameter are launched at various radial positions in the gas flow field. In order to compare the simulation with the experiment for NaCl particles, the particles in the simulation are assumed to be spherical NaCl particles with

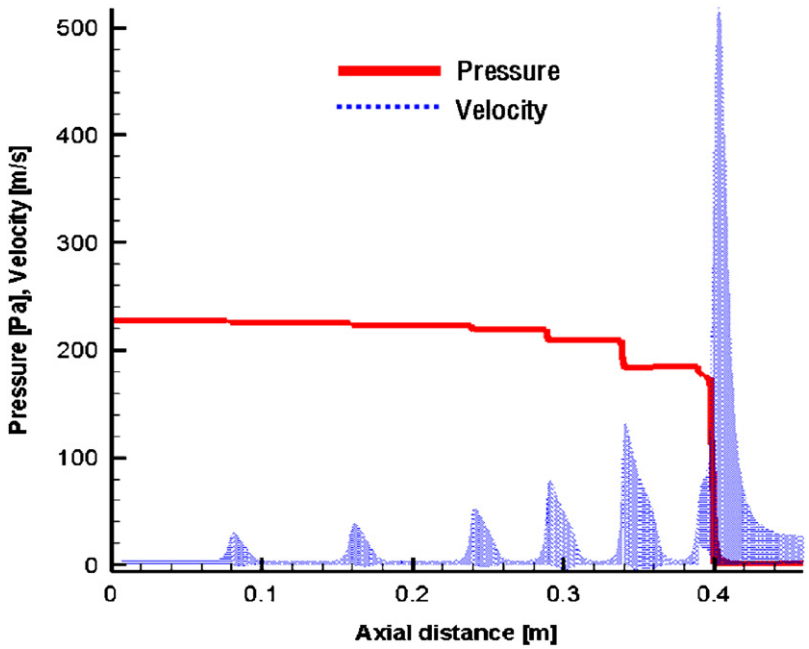

Fig. 4. Pressure drop and streamwise velocity of gas flowing through the series of orifices: $Q = 125$ sccm.

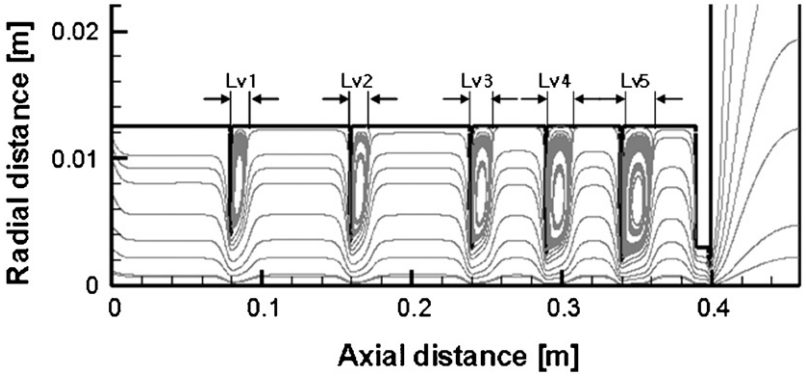

Fig. 5. Gas flow streamlines in the multi-lens assembly: $Q = 125$ sccm.

a density of ~ 2 g/cc. By solving the Langevin equation including inertia and drag forces (Liu et al., 1995a; Wang, Gidwani et al., 2005; Wang, Kruis et al., 2005, Zhang et al., 2002, 2004), we could simulate particle trajectories through the entire ADL system.

As the particle size of interest in this study ranges from 30 to 300 nm, we do not include in the calculation the Brownian motion of particles that has a significant effect especially for the size smaller than 30 nm (Wang, Gidwani et al., 2005). Liu et al. (1995a) showed that if particles are initially close to the centerline of the lens, the initial radial positions of particles do not affect the performance of the lens. As almost 50% of particles exhibit this so-called near-axis behavior in this study, we restrict the presentation only for the near-axis particles as many researchers have done before (Liu et al., 1995a; Wang, Gidwani et al., 2005; Wang, Kruis et al., 2005; Wang & McMurry, 2006b; Zhang et al., 2002, 2004).

3.1. Dimensionless parameters and their relationship

The performance of the ADL or the single lens has been often represented by overall contraction ratio (η_c) of particle beam and transmission efficiency (η_t) of particles. Zhang et al. (2002) suggested that the two factors were characterized as a function of four dimensionless groups such as d_f/OD, L/d_f, flow Reynolds number (Re_0) based on the OD and particle Stokes number (St) as

$$\begin{aligned} \eta_c &= f(d_f/\mathrm{OD}, L/d_f, Re_0, St), \\ \eta_t &= g(d_f/\mathrm{OD}, L/d_f, Re_0, St), \end{aligned} \tag{1}$$

where d_f is the size of orifice opening, OD is outer diameter of the orifice and L is the length of the spacer. As mentioned earlier in the section of experiment, the pressure inside the ADL is so low that gas mean free path is much larger than 300 nm (the largest particle size of interest). The particle behavior in this condition is supposed to be in the free molecular regime. In the regime, the St can be defined using Epstein's mobility as (Liu et al., 1995a; Wang, Kruis et al., 2005)

$$St = \frac{1}{(1+\pi\alpha/8)\sqrt{2\pi\gamma^3}} \frac{\dot{m}\rho_p d_p c^3}{p_{up}^2 d_f^3} \propto \frac{\rho_p d_p}{p_{up}^2 d_f^3 M^{3/2}}, \tag{2}$$

where α is the momentum accommodation coefficient (close to the unity), γ is the specific heat ratio of the gas (1.4 for air), ρ_p is particle density, d_p is particle diameter, $c = \sqrt{\gamma R T_{up}/M}$ is the speed of sound in the gas at the upstream temperature (T_{up}), M is molecular weight of the gas and $\dot{m}$ is mass flow rate of carrier gas.

Even if Re_0 remains constant at different d_f's (constant OD and $\dot{m}$), the characteristics of gas flow and particle behavior are still affected by the lens geometric factor d_f. Also, Zhang et al. (2002) did not consider Mach number (Ma) as a dimensionless parameter in Eq. (1) under the assumption of very low Ma. This is true only when $Ma < 0.10$ (see Wang & McMurry, 2006b, Fig. 3). But in many practical conditions, the Ma is out of range (will be seen). According to Eq. (1), they seem to have too many (four or five) design parameters that can be independently changed.

In Zhang et al. (2002), it is therefore often seen that the curves of η_c versus St at different d_f/OD were not collapsed into a single curve. Due to the complexity, they could not find out the functional relationship for optimal Stokes number (St_0) when $\eta_c = 0$. The lack of knowledge of the St_0 at each orifice made it impossible to determine the optimal orifice diameters (d_{f0}) (see Eq. (6)). This is why their multi-lens system could not be optimized.

The gas flow should be better characterized by the other Reynolds number based on the d_f rather than the OD as

$$Re = \frac{\rho_{up} V_f d_f}{\mu} = \frac{4\dot{m}}{\pi \mu d_f} \propto \frac{1}{d_f}, \tag{3}$$

where μ is gas viscosity, ρ_{up} implies the gas density upstream of each orifices and V_f stands for the gas velocity estimated with respect to the ρ_{up} : $V_f = \dot{m}/(\rho_{up} A_f)$. The $\dot{m}$ is maintained constant throughout all orifices and defined as (Wang & McMurry, 2006b)

$$\dot{m} = \rho_{up} V_f A_f = A_f \frac{C_d Y}{\sqrt{1-\beta^4}} \sqrt{2\rho_{up}\Delta P} = A_f \frac{C_d Y}{\sqrt{1-\beta^4}} P_{up} \sqrt{\frac{2RT_{up}\Delta P}{P_{up} M}}, \tag{4}$$

where C_d is a discharge coefficient through an orifice that is known as a function of the Re, β is the constriction ratio of a thin orifice ($=d_f$/OD) the ΔP is a pressure drop across the orifice, and the Y is expansion factor known as a function of the pressure ratio $\Delta P/P_{up}$ (Wang & McMurry, 2006b).

If the d_f decreases, the Re and St are both increased (see Eqs. (2) and (3)), leading to significant changes in both gas flow characteristics and particle behavior. At the same time, the P_{up} is expected to increase because the pressure downstream of the nozzle exit (P_{dn}) is fixed constant during the operation of the SPMS. The higher P_{up} condition reduces the detrimental effect of particle diffusion. More importantly, as the OD is often restricted geometrically for the application to the SPMS, the lens-geometry-related parameter (d_f/OD) would be reduced to the Re (see Eq. (3)). The length L of the spacer is not a big concern for the design as long as the L is long enough for the gas flow to redevelop after the orifice. In all these respects, Eq. (1) is likely reduced to the simpler form as

$$\eta_c = f_1(Re, St), \quad \eta_t = g_1(Re, St). \tag{5}$$

At the fixed d_f and $\dot{m}$, where Re is constant (see Eq. (3)), η_c must be determined solely by St. But the ADL system consisting of orifices with the same d_f is well known to be much less effective. When $\eta_c = 0$ in Eq. (5) (say, corresponding to the best design), St_0 seems to be related only to Re : $St_0 = f_2(Re)$. If the functional relationship f_2 is known, St_0 is easily determined from Re. By rearranging Eq. (2) for d_f, the optimal orifice size (d_{f0}) of each orifice is given directly from St_0 as

$$d_{f_0} = \frac{1}{(1+\pi\alpha/8)^{1/3}(2\pi\gamma^3)^{1/6}} \left(\frac{\dot{m}\rho_p d_{p0} c^3}{p_{up}^2 St_0} \right)^{1/3}, \tag{6}$$

where d_{p0} implies the optimal size of particles to be best focused at the orifice. Let us explain the physical meaning of d_{p0}. Fig. 6 shows that particles smaller than d_{p0} are not efficiently focused while larger particles ($> d_{p0}$) are overfocused due to their greater inertia.

But, in reality, the optimal design is not so easy because St_0 and the relation f_2 are both unknown yet. When $Ma > 0.10$, as described before, Ma should be added as a parameter to Eq. (5):

$$\eta_c = f_3(Re, St, Ma), \quad \eta_t = g_3(Re, St, Ma). \tag{7}$$

Accordingly, the relation between St_0 and other parameters (f_2) should be changed to

$$St_0 = f_4(Re, Ma). \tag{8}$$

Wang and McMurry (2006b) are the only researchers who attempted to obtain f_4. Unfortunately they failed to extract the functional form of f_4. Instead, they calculated St_0 as a function of Re at three different Mach numbers for single lens. Note that they treated Ma as independent variable with respect to Re. Is this true? If Ma has a functional dependence

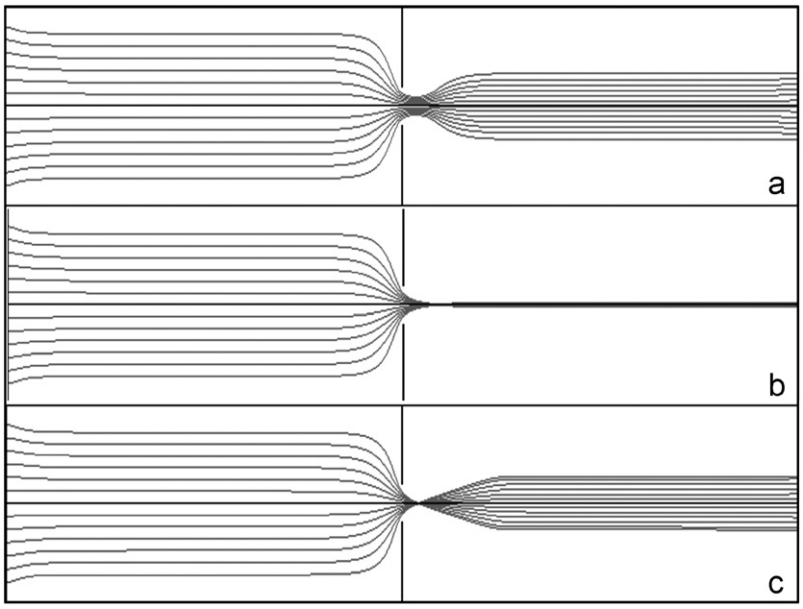

Fig. 6. Particle size-dependent focusing of single lens: (a) insufficient focusing smaller particles ($d_p = 30$ nm), (b) focusing intermediate sized particles ($d_p = 150$ nm), (c) overfocusing larger particles ($d_p = 500$ nm): $Q = 125$ sccm.

on Re, St_0 would be expressed as a sole function of Re. To check this, let us go back to the definition of Ma. Ma is defined as the ratio of V_f to sound speed (c) at upstream temperature T_{up}:

$$Ma = \frac{V_f}{c} = \frac{\dot{m}}{A_f}\frac{1}{P_{up}}\sqrt{\frac{RT_{up}}{\gamma M}} = \frac{C_d Y}{\sqrt{1-\beta^4}}\sqrt{\frac{2\Delta P}{\gamma P_{up}}}, \tag{9}$$

where γ is specific heat ratio of the gas. Flow velocity at the orifice throat (V_f) is a common factor in the definitions of Re and Ma (see Eqs. (3) and (9)). If the d_f of an orifice decreases at constant downstream pressure, the upstream density ρ_{up} increases along with increases in P_{up} and V_f, leading to increase in Re and Ma. Thus, the Ma has a functional dependence on Re. By combining Eqs. (3), (4) and (9), the relationship between Re and Ma is given as

$$Re = \frac{\rho_{up} V_f d_f}{\mu} = \frac{4\dot{m}}{\pi\mu d_f} = \frac{d_f P_{up}}{\mu}\frac{C_d Y}{\sqrt{1-\beta^4}}\sqrt{\frac{2\Delta P}{P_{up}}}\sqrt{\frac{M}{RT_{up}}} = Ma\ d_f P_{up}\frac{1}{\mu}\sqrt{\frac{\gamma M}{RT_{up}}}. \tag{10}$$

Since d_f in the right hand side of Eq. (10) is inversely proportional to Re (see Eq. (3)), the substitution of d_f as a function of Re to Eq. (10) gives a more clear functional relationship between Ma and Re:

$$Ma = \frac{Re^2}{P_{up}}\frac{\pi\mu^2}{4\dot{m}}\sqrt{\frac{RT_{up}}{M}}. \tag{11}$$

Eq. (11) shows that given the constant $\dot{m}$, Ma is linearly proportional to Re^2/P_{up}.

Note that P_{up} is only dependent on Re and d_f/OD (or OD) from Eq. (4) in practical condition ($\dot{m}$ and P_{dn} are constant). Thus, Eq. (11) shows that Ma is also a function of Re and OD. By substituting this into Eqs. (7) and (8), the equations are rewritten in simpler forms:

$$\eta_c = f_5(Re, St, OD), \quad \eta_t = g_5(Re, St, OD), \tag{12}$$

$$St_0 = f_6(Re, OD). \tag{13}$$

Table 1
Comparisons of design parameters between the present design and the previous ones at $Q = 125$ sccm

Lens order	d_f	d_f/OD	Ma	Re	P_{up} (Pa)	d_{po} (nm)	St_0
Present design							
OD (mm)	25						
1	8	0.32	0.086	22.48	227.2	750	1.036
2	7	0.28	0.112	25.69	225.6	390	0.816
3	6	0.24	0.155	29.97	223.2	210	0.713
4	5	0.2	0.228	35.97	218.6	105	0.642
5	4	0.16	0.386	44.96	209.2	43	0.561
Zhang et al. (2004)							
OD (mm)	12						
1	5	0.416	0.19	39.965	274.4	none	none
2	4.8	0.4	0.218	37.463	266.3	300	1.397
3	4.5	0.375	0.255	39.961	256.8	180	1.094
4	4.3	0.358	0.298	41.819	244.3	115	0.885
5	4	0.333	0.38	44.956	229	70	0.761
Liu et al. (1995a)							
OD (mm)	10						
1	5	0.5	0.17	35.965	305	none	none
2	4.5	0.45	0.222	39.961	297	none	none
3	4	0.4	0.295	44.956	286	170	1.186
4	3.75	0.375	0.365	47.953	268	100	0.964
5	3.5	0.35	0.485	51.378	243.5	50	0.718

Hence, three parameters such as Re, Ma and P_{up} are interrelated and affected by lens geometry (d_f and OD) and systematic factors ($\dot{m}$ and P_{dn} or downstream pressure). The parameters must not be treated as independent variables as done before by Zhang et al. (2002) and Wang and McMurry (2006a, 2006b). For instance, the P_{up} of an orifice should be matched with the downstream pressure of the preceding orifice. This is why full numerical calculations should be made for the entire ADL system so as to predict correct values of the parameters.

3.2. Design of the ADL system

Let us address how the designing process is going. As mentioned earlier, the values of $\dot{m}$, OD, and P_{dn} (the pressure downstream of the nozzle exit) are all fixed for the purpose of the ADL as an inlet of the SPMS. This makes the design process much simpler. First, we choose the total number of lenses and the size range of particles to be focused. If the lens number is increasing, size-polydisperse particles are more precisely focused. But this increases the total length of the ADL inlet. The spacer separating two successive orifices should have a sufficient length (L) for allowing the gas flow to redevelop completely. In Fig. 3, the ADL is assembled to the precise manipulator that is mounted 300 mm upstream of the center of the first chamber. Regarding this and the minimum L, we set the total length to be long enough to install five lenses. Each of the lenses is going to be designed to focus particles having different sizes.

In Fig. 3, the P_{up} is varied not so much that it is first approximated to be constant throughout the ADL. Liu et al. (1995a) reported that when $d_f/\mathrm{OD} < 0.25$, the St_0 had a weak dependence on the ratio. In the present condition, the OD is set to be 25 mm under the consideration of the adapter size of the SPMS. The relatively large OD offers several benefits such as more options for selection of d_f and a wider size range of the focusable particles. According to Wang and McMurry (2006b), St_0 is varied only from 0.5 to 1.0 when $0.03 < Ma < 0.32$. It is therefore plausible to first approximate St_0 to be constant with a value in the range. Then Eq. (6) implies that d_{p0} is proportional to the cubic power of d_{f0} ($d_{p0} \propto d_{f0}^3$). When d_f decreases at a uniform interval (e.g., 1 mm) to the streamwise direction as shown in Fig. 2, the decrement of d_{p0} decreases faster (see the present design in Table 1). The purpose of this scheme is as follows. Large particles being effectively focused need only one or two successive lenses, whereas smaller ones to be focused inefficiently require more near-optimal stages of the lenses for better focusing.

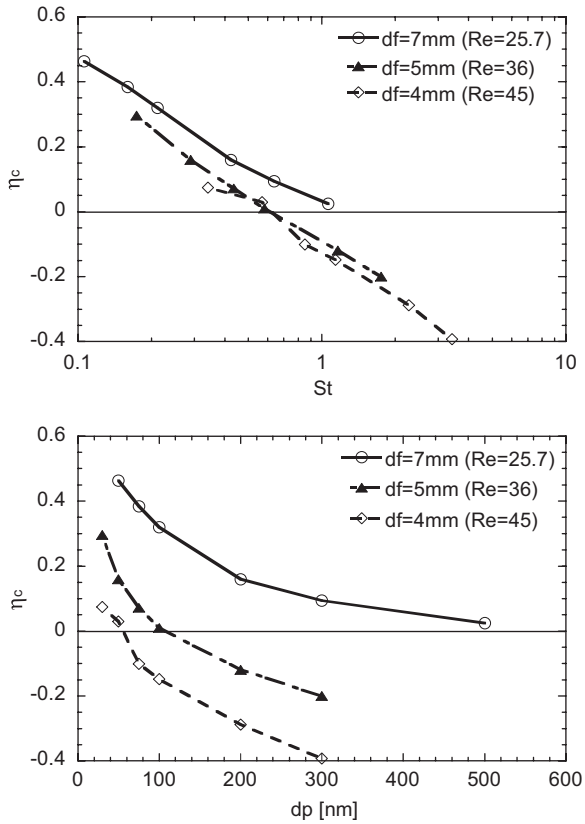

Fig. 7. Comparisons of contraction ratios at the 2nd, 4th, and 5th lenses as a function of (a) Stokes numbers and (b) particle diameters : $Q = 125$ sccm.

Once all lenses are initially specified (d_f), the other parameters such as Re, P_{up} and Ma can be obtained from Eqs. (3), (4), and (9) (or (11)), respectively. But, in this design, we instead calculate those values directly from the full numerical simulations. If either the value of St_0 or the function of f_4 in Eq. (8) (f_6 in Eq. (13) as an alternative) is known, d_{f0} is updated at each orifice from Eq. (6) and the targeted particle sizes (d_{p0}). With the updated set of the d_f's, the process is then iterated until all values of the d_{f0}'s are converged. The process is somehow similar to that used in the design tool of Wang and McMurry (2006b). But note that they used the simple equations such as Eqs. (4), (6), (9), and (10) to calculate the parameters. This results in some overestimation for P_{up} at all orifices, leading to overestimation in the optimal particle size d_{p0}. A more significant difference is put forward to obtain St_0. We will discuss it in detail later.

Using this scheme, we design and fabricate the present ADL shown in Fig. 2 with the purpose of focusing the 30–700 nm particles. We test the entire ADL system by the full numerical simulation. Fig. 7(a) shows that St_0 is not varied much around 0.6 from the 3th orifices to the 5th. But the 1st and 2nd orifice diameters give the d_f/OD of 0.32 and 0.28, respectively, which are larger than the critical value of 0.25 by Liu et al. (1995a). Therefore, the universality of St_0 is broken especially at these two orifices, moving St_0 to 1.0. All the necessary parameters for the present design are listed in Table 1. Transmission efficiency of particles is also calculated as a function of St at all orifices and nozzle. As an example, we compare the η_t vs St curves at the 3rd orifice and nozzle in Fig. 8. It should be noted that under typical operating conditions ($0.1 < St < 10$), all lenses including the nozzle can penetrate almost 100% of 15–700 nm particles in the multi-lens system.

Here, let us remind that the purpose of this study was to develop an efficient ADL inlet of the SPMS. Therefore, for better evaluation of the inlet, the overall transmission efficiency and the particle beam diameter are calculated 210 mm downstream of the ADL exit (at the ionization region). In addition, we consider two aerosol-gas flow rates of 125 and 210 sccm upstream of the flow limiting orifice. The use of a smaller mass flow rate or a smaller flow limiting orifice

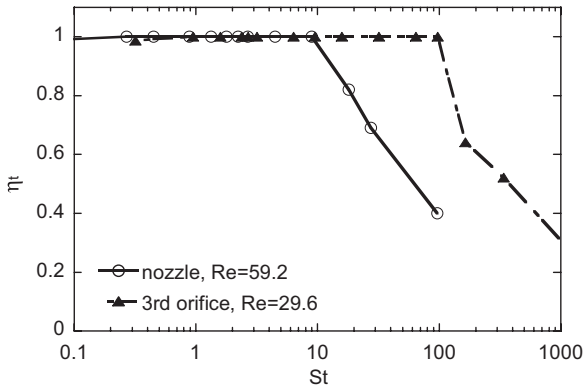

Fig. 8. Comparisons of transmission efficiency at the 3rd orifice and nozzle as a function of the St : $Q = 125$ sccm.

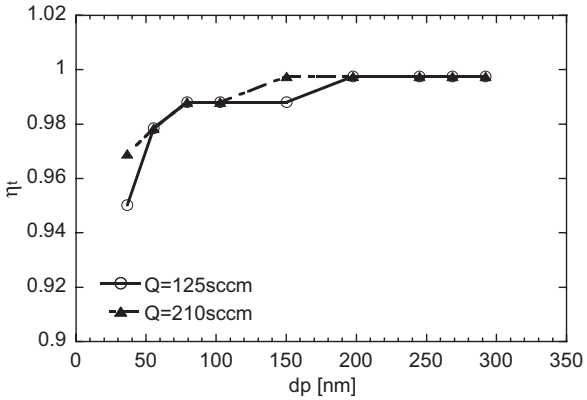

Fig. 9. Overall transmission efficiencies calculated for two flow rates of gas entering the ADL system.

provides an advantage of focusing smaller particles. That is, this decreases all upstream pressures inside the ADL, thereby leading the St for the smaller particles to approaching the optimal value of St_0. But this would be achieved at the expense of the hitting rate by the SPMS. Fig. 9 shows again the present ADL system can deliver particles in the size range of interest (30–300 nm) with almost 100% efficiency at both gas flow rates.

The St is always smaller than 10 in our design, implying that the inertia loss of large particles is not a concern. Brownian diffusion is not considered. The transport efficiency therefore should not be varied with decreasing particle size. But why does η_t decrease as d_p decreases? This is the sort of artifacts occurring at the simulation of particle trajectories. We release as many as 200–1000 particles for more accurate calculation of the trajectories. In this case, FLUENT often restricts the total calculation time due to memory limit of the computer. Therefore, while particles staying near axis and moving faster arrive at the destination where η_t is measured, near-wall particles cannot arrive at their destination and be regarded as being lost. This is more pronounced for smaller particles flying with lower speed and higher gas flow rates.

Fig. 10 presents the trajectories of aerosol particles of 50, 100, and 300 nm for the two gas flow rates. The final aerosol beam diameters are estimated 40 mm downstream of the ADL exit. Fig. 10(a) shows 50 nm particles are collimated at the 5th nozzle, but 300 nm particles are completely focused between the 2nd and 3rd orifices. We would like to emphasize that the final beam diameters are still in the sub-millimeter range for $Q = 125$ sccm.

Now, we would compare the performance of the present design with that of the previous designs. We performed similar studies for Liu et al.'s and Zhang et al.'s designs. The resultant parameters of interest are all compared in Table 1. The blank represents that St_0 does not exist. The characteristics of each design are clearly indicated in the

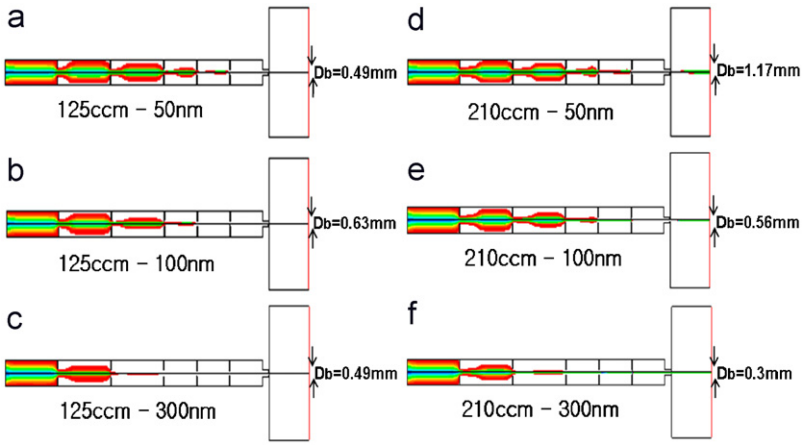

Fig. 10. Trajectories of particles with a variety of their sizes at two gas flow rates.

column of optimal particle size (d_{p0}) of the table. Among the three designs, the present design is the only one capable of focusing particles from 30 to 750 nm.

3.3. Optimization using the design tool

The design tool supplied by Wang and McMurry (2006b) is obviously useful for anyone who does not know the numerical simulation. He/she can have shortly the near optimal design that is suitable for their purpose. This benefit leads many researchers to use the tool without any detailed investigation. Here, we would like to address the physical significances of two approximations that have not been clarified yet.

3.3.1. Errors for prediction of the optimal Stokes numbers

Wang and McMurry (2006b) failed to obtain the functional form of f_4 in Eq. (8). How could they then develop the design tool for optimization of the lens design? The answer is as follows. They calculated St_0 as a function of Re at three different Mach numbers (0.03, 0.1, and 0.32) only from single-lens analysis. When using the design tool, one may have to predict the St_0 at any pair of Ma and Re (i.e., at a certain lens). The prediction was made through interpolation and extrapolation with three vertical points at a given Re (refer to Fig. 3 in their paper). For example, when $Ma = 0.2$ and $Re = 20$, they took a value between $St_0 = 0.8$ at $Ma = 0.1$ and $St_0 = 0.6$ at $Ma = 0.32$ by the interpolation (refer to the Visual Basic code linked to the design tool). In the three different designs in Table 1, the Ma varies from 0.09 to 0.485 along the orifices, even excluding the nozzle region. As an extrapolation often gives a considerable error, the prediction of St_0 is likely incorrect especially at relatively high Ma positions. The error is expected to be more noticeable for smaller particles because those particles are more easily affected by the undesired gas flow. The correct estimation of St_0 is therefore one of the key design factors.

3.3.2. Other minor errors

Fig. 3 in Wang and McMurry (2006b) was obtained for a single lens of $d_f/\mathrm{OD} = 0.2$. What will happen if the ratio deviates from the value of 0.2? To answer the question, we calculated the St_0 at various conditions by a number of FLUENT simulations. We design and test four more different 5-lens systems. Following our scheme, the first two trials (Test # 1 and 2) are designed at the two different ODs. The other two trials (Test # 3 and 4) are considered to know the effect of the OD by only changing the value of OD in the each design of Zhang et al. and Liu et al. Hence, we have seven different designs. The simulation results and detail lens geometries for the four cases are summarized in Table 2 in terms of the parameters of interest.

Under the same conditions, the optimal Stokes numbers in the table are compared with the values predicted by Wang and McMurry (2006b). Fig. 11 shows that their predictions of St_0 are almost correct at low β ($=d_f/\mathrm{OD}$), where St_0 is

Table 2
Design characteristics of four trials made in this study at $Q = 125$ sccm

Lens order	d_f	d_f/OD	Ma	Re	P_{up} (Pa)	d_{po} (nm)	St_0
Test #1							
OD (mm)	18						
1	7	0.39	0.11	25.69	239.6	760	1.409
2	6.5	0.36	0.128	27.67	237.2	500	1.181
3	6	0.33	0.153	29.97	234	300	0.926
4	5	0.28	0.226	35.97	229.6	125	0.693
5	4	0.22	0.386	44.6	220.5	50	0.587
Test #2							
OD (mm)	12						
1	4.5	0.38	0.167	39.96	384.2	370	1.004
2	4	0.33	0.218	44.96	376	200	0.807
3	3.5	0.29	0.302	51.38	363.2	105	0.678
4	3	0.25	0.462	59.94	340	46	0.538
5	2.8	0.23	0.714	64.22	292	24	0.468
Test #3–Zhang et al.'s lens modified (OD 10–25 mm)							
OD (mm)	25						
1	5	0.2	0.193	39.965	256	162	0.722
2	4.8	0.192	0.218	37.463	248	127	0.682
3	4.5	0.18	0.255	39.961	238.3	95	0.67
4	4.3	0.172	0.3	41.819	225.5	72	0.65
5	4	0.16	0.386	44.956	209	45	0.588
Test #4–Liu et al.'s lens modified (OD 10–25 mm)							
OD(mm)	25						
1	5	0.2	0.172	35.965	286.2	208	0.742
2	4.5	0.18	0.215	39.961	279.2	138	0.709
3	4	0.16	0.29	44.956	268.5	86	0.681
4	3.75	0.15	0.365	47.953	250	60	0.665
5	3.5	0.14	0.476	51.378	224	38	0.645

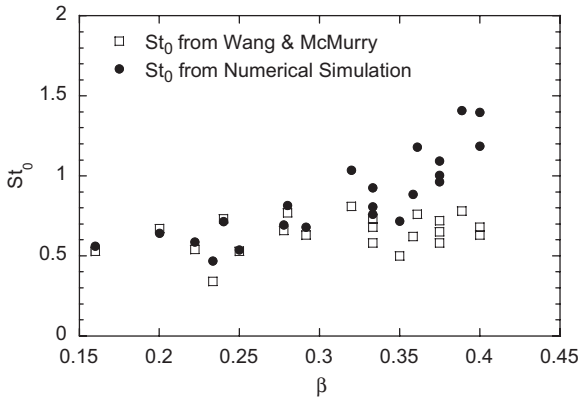

Fig. 11. Error in the prediction of St_0 made by Wang and McMurry (2006b).

not varied with β (Liu et al., 1995a). When $\beta > 0.25$, they begin to underestimate St_0 and the error becomes greater. Let us note from Eq. (6) that the error for St_0 is exactly transferred to the error in d_{p0}.

Wang and McMurry (2006b) suggested that the pressure upstream of each orifice (P_{up}) is a very important parameter to control the gas and particle behavior. They derived several approximated relations to avoid full numerical calculation.

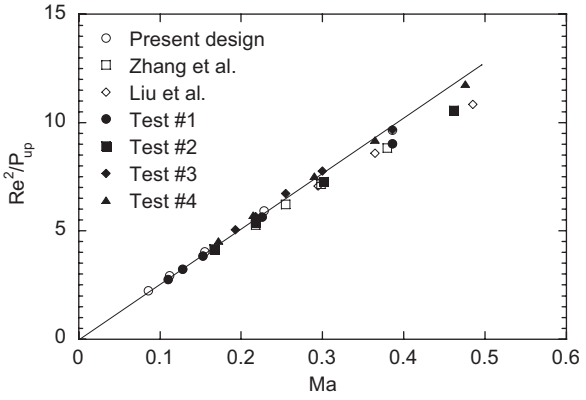

Fig. 12. Linear correlation between Re^2/P_{up} and Ma.

Using the equations, they numerically iterate to solve P_{up} and other parameters at the last orifice with a fixed or obtained pressure upstream of nozzle. All upstream pressures at the other preceding orifices are subsequently obtained to the reverse-streamwise direction. Though this gives a great opportunity to reduce the time and cost for the simulation, the final error after convergence might not be negligible due to the iteration for several approximated equations. We compared the values in Tables 1 and 2 with those estimated by running their tool (not shown here). In the case of the small OD, the error is definitely negligible; however, the tool overestimates P_{up} by 10% at the largest OD of 25 mm. Recalling Eq. (6) in this case, the almost 20% overprediction of d_{p0} is expected.

3.4. Universal correlation of optimal Stokes number with other parameters

All results in Tables 1 and 2 are obtained under the constant values of $\dot{m}$ and P_{dn}. We have now enough data sets to extract any statistically meaningful trend. Remember that Eq. (11) indicates that Ma is directly proportional to Re^2/P_{up}. Here, it is interesting to check whether or not all our results satisfy the relationship. Interestingly, Fig. 12 shows that the two parameters have an almost linear relationship.

Let us consider the case of increasing OD with no change in other lens geometries and parameters. In this case, it is noticeable that ΔP in Eq. (6) is mainly dependent on d_f and does not vary with OD. This is verified by comparing the values of ΔP between Zhang et al.'s result in Table 1 and Test #3 in Table 2. As Re in the equation is constant, the only variant terms are P_{up} ($\propto 1/\mathrm{Ma}$) and β (or OD). Under the condition of the larger OD, the accelerated gas flow at each orifice throat should consume more energy to expand more, leading to bigger pressure drop. This would happen at all kinds of throats including the flow limiting orifice. This is why all values of P_{up} decrease as OD increases independently (compare again the results of Zhang et al. and Test #3 in the tables).

Though the decrement of P_{up} is as small as 10% or less, it is expected to generate a considerable increase of St, because St is inversely proportional to $1/P_{up}^2$ (see Eq. (2)). This is the intrinsic effect of OD on particle behavior through Ma or P_{up}. In order to include the effect of OD, we add constriction ratio β to Eq. (7) as $\eta_c = f_7(St, Re, Ma, d_f/\mathrm{OD})$. Accounting for (10) and (11), this is rewritten as

$$\eta_c = f_8(St, Re, Re^2/P_{up}, d_f/\mathrm{OD}) = f_9(St, Re, P_{up}, d_f/\mathrm{OD}) = f_{10}(St, Re, P_{up}, \mathrm{OD}). \tag{14}$$

In this condition, Eq. (4) indicates P_{up} is expressed as a function of Re and OD. Consequently, function f_{10} can be more simplified and reduced to Eqs. (12) and (13) as

$$\eta_c = f_{11}(St, Re, \mathrm{OD}),$$
$$St_0 = f_{12}(Re, \mathrm{OD}). \tag{15}$$

From Eq. (10) it is observed that the term of $Re/P_{up}/Ma$ scales as the characteristic length (d_f) of orifice. Therefore, the ratio of $(Re/P_{up}/Ma)/\mathrm{OD}$ might correspond to a single integrated parameter determining the particle behavior. All the values of St_0 in the seven designs are plotted against the integrated parameters. For the best correlation, we

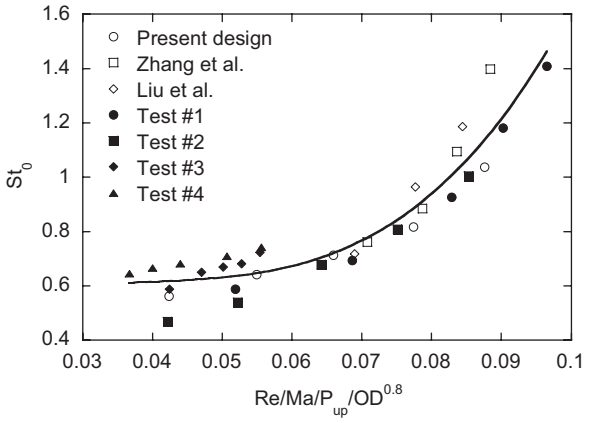

Fig. 13. A universal correlation of the St_0 with $Re/Ma/P_{\mathrm{up}}/\mathrm{OD}^{0.8}$.

vary the power of OD around 1.0 in the single parameter. As a result, the power of 0.8 for OD is discovered to produce a good correlation. Fig. 13 shows that the St_0 is expressed nearly by a single function (cubic power) of $Re/P_{\mathrm{up}}/Ma/\mathrm{OD}^{0.8}$. Using the near universal correlation, one might be able to estimate the optimal Stokes numbers better than the interpolation or extrapolation. Also the correlation is expected to replace the part of the interpolation used in the subroutine. Taking a close look at the parameter, one can reduce it to a simpler form. The product of Ma and P_{up} scales as Re^2 for the constant $\dot{m}$ (see Eq. (11)). Then, the x-axis of $Re/Ma/P_{\mathrm{up}}/\mathrm{OD}^{0.8}$ in the figure can be converted to $1/Re/\mathrm{OD}^{0.8}$. This is again consistent with Eq. (15).

4. Experimental evaluation of the ADL system

We first visualize the particle beam by light scattering measurement. Fig. 14(a) shows a photograph of the aerosol beam formed under vacuum, while Fig. 14(b) is a similar scattered image for indoor dust entrained to the 2nd chamber on pumping off. The latter photograph is taken at atmosphere to show how large the scattering laser beam is. It is obvious that the scattering laser beam encompasses the particle beam. We also crosscheck this by moving the ADL system with respect to the fixed laser beam. If the laser beam begins to partly overlap the aerosol beam, the visualized aerosol beam gets narrower. Note that Fig. 14(a) corresponds to the largest image of aerosol beam taken 210 mm downstream of the ADL exit (the center of the 2nd chamber). To the best of our knowledge, this would be the first visualization of the aerosol beam formation in the ADL inlet of the SPMS. However, we have to mention that the aerosol particles are not size-selected by a differential mobility analyzer (DMA), because such a size selection dilutes particle concentration too much to obtain a clear scattering image. Nevertheless, it is worthwhile to see that the diameter of the collimated aerosol beam is still in the sub-millimeter range even at the position of the ionization laser.

After size selecting particles with a DMA, we deposited an aerosol beam of those particles to a substrate 40 mm downstream of the lens exit. The distance of 40 mm is largest in the SPMS with no significant disintegration of its vacuum components. Fig. 15 shows some images of the deposited layers. It is obvious that larger particles are better focused, which is qualitatively consistent with Fig. 10. We would like to note that the blurred backgrounds surrounding a very bright white sphere in Figs. 15(c) and (d) are not caused by less particles existing at the surrounding. We observed that the brightness of the surrounding part is greatly changed while rotating the bulb of the optical microprobe. At this time, the core part is, however, not changed in brightness. Therefore, the blurred background in the image is thought as the bulb light reflected on the three-dimensional layer. Note that the layer of 100 nm particles does not show such background and the core part is not as bright as in Figs. 15(c) and (d). This implies that the layer of larger particles is taller and denser than that of smaller particles. For a quantitative evaluation of the ADL system, the aerosol beam diameters predicted from the simulations are compared with those measured from the deposition and observation experiment. Fig. 16 shows that the numerical predictions agree reasonably well with those of the experiment for almost all conditions considered in this study.

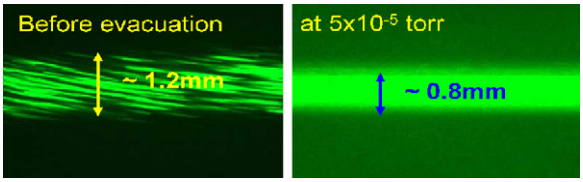

Fig. 14. The scattered images captured before evacuation and under vacuum.

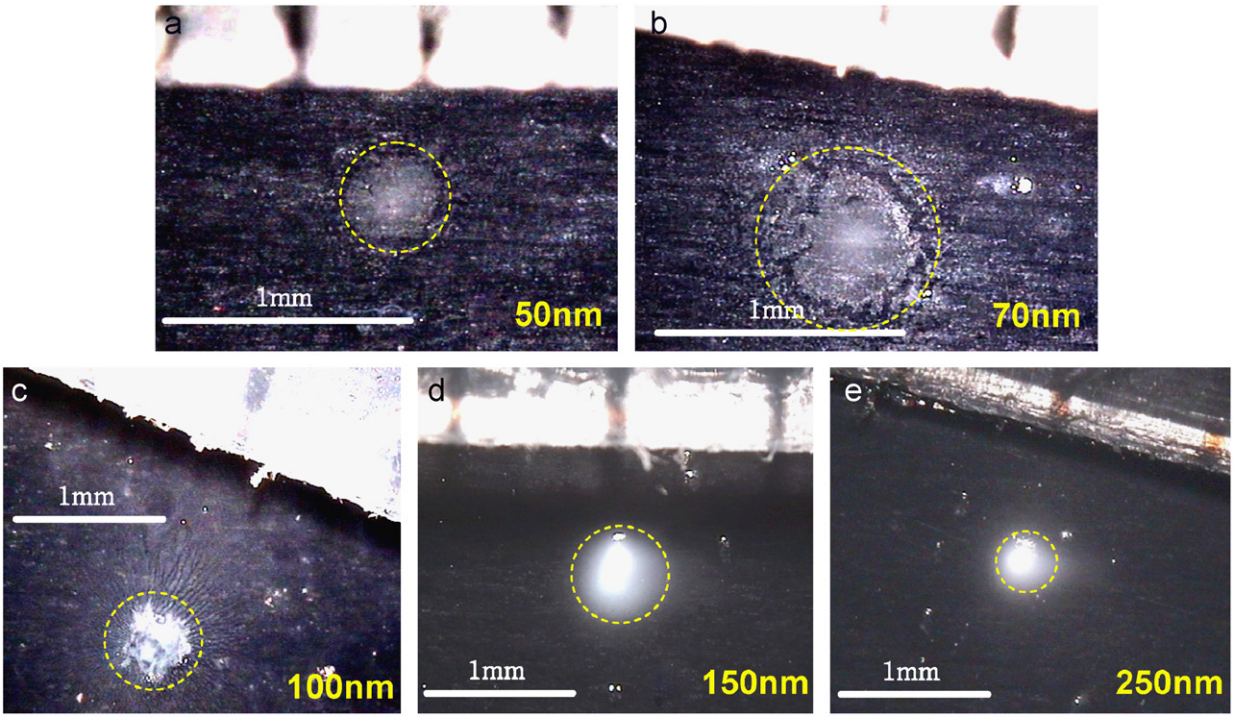

Fig. 15. Observation of the deposited layer of aerosol particles with the specified sizes. The bar represents 1 mm in length and a ruler was positioned at the top of the images for comparisons.

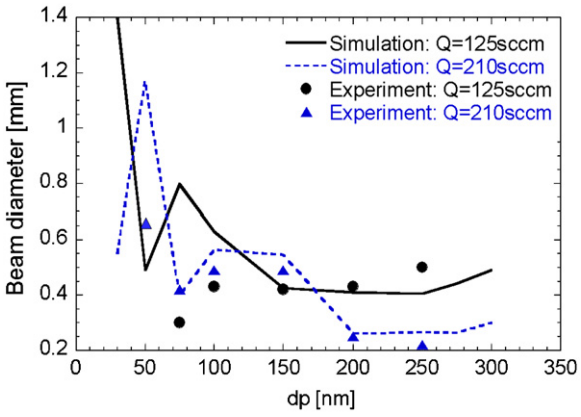

Fig. 16. Comparisons of aerosol beam diameters between experiments and numerical predictions.

5. Conclusions

In this study, we attempted to understand several dimensionless parameters and systematic factors for designing an efficient aerodynamic lens, using full numerical simulations for the whole lens system. Seven different designs of the system are investigated. We found particle behavior was mainly determined by two dimensionless parameters such as particle Stokes number and flow Reynolds number. Mach number was not an independent parameter but interrelated well with flow Reynolds numbers and pressures upstream of the orifices. By manipulating the parameters, we showed for the first time a possibility that there exists a universal correlation between optimal Stokes number and a new factor incorporating the other dimensionless variables and a design parameter. The universality was confirmed by the full simulation results. Only with the help of the correlation, we can reduce some potential errors that arise from the prediction of the optimal Stokes number. We demonstrated that the new design of the system was capable of focusing ultrafine aerosols in the size range of 30–700 nm. Two methods such as light scattering imaging and deposition/microprobe observation were successfully used to visualize the tightly focused aerosol beams. These have not been achieved before. Finally, the diameters of particle beams predicted by numerical simulations agreed reasonably well with those measured by the experiment.

Acknowledgments

This work was supported by Core Environmental Technology Development Project for the Next Generation (Project No. 102-071-058).

References

Carson, P. G., Johnston, M. V., & Wexler, A. S. (1997). Laser desorption/ionization of ultrafine aerosol particles. *Rapid Communications in Mass Spectrometry*, *11*, 993–996.

Cheng, Y. S., & Dahneke, B. E. (1979). Properties of continuum source particle beam II. Beams generated in capillary expansions. *Journal of Aerosol Science*, *10*, 363–368.

Cho, S.-W., & Lee, D. (2007). An ion optics for effective ion detection in single particle mass spectrometry. *Rapid Communications in Mass Spectrometry*, *21*(20), 3286–3294.

Dahneke, B. E., & Cheng, Y. S. (1979). Properties of continuum source particle beam. I. Calculation methods and results. *Journal of Aerosol Science*, *10*, 257–274.

Fonzo, F. D., Gidwani, A., Fan, M. H., Neumann, D., Iordanoglou, D. I., Heberlein, J. V. R. et al. (2000). Focused nanoparticle-beam deposition of patterned microstructures. *Applied Physics Letter*, *77*(6), 910–912.

Huffman, J., Jayne, J., Drewnick, F., Aiken, A., Onasch, T., Worsnop, D. et al. (2005). Design, modeling, optimization, and experimental tests of a particle beam width probe for the aerodyne aerosol mass spectrometer. *Aerosol Science and Technology*, *39*, 1143–1163.

Israel, G. W., & Friedlander, S. K. (1967). High speed beams of small particles. *Journal of Colloid and Interface Science*, *24*, 330–337.

Jayne, J. T., Leard, D. C., Zhang, X. F., Davidovits, P., Smith, K. A., Kolb, C. E. et al. (2000). Development of an aerosol mass spectrometer for size and composition analysis of submicron particles. *Aerosol Science and Technology*, *33*(1–2), 49–70.

Kane, D. B., & Johnston, M. V. (2000). Size and composition biases on the detection of individual ultrafine particles by aerosol mass spectrometry. *Environment Science and Technology*, *34*(23), 1887–4893.

Katrib, Y., Martin, S., Rudich, Y., Davidovits, P., Jayne, J., & Wornop, D. (2005). Density changes of aerosol particles as a result of chemical reactions. *Atmospheric Chemistry and Physics*, *5*, 275–291.

Lee, D., Miller, A., Kittelson, D., & Zachariah, M. R. (2006). Characterization of metal-bearing diesel nanoparticles using single particle mass spectrometry. *Journal of Aerosol Science*, *37*(1), 88–110.

Lee, D., Park, K., & Zachariah, M. R. (2005). Determination of size distribution of polydisperse nanoparticles with single particle mass spectrometry: The role of ion kinetic energy. *Aerosol Science and Technology*, *39*, 162–169.

Liu, P., Ziemann, P. J., Kittelson, D. B., & McMurry, P. H. (1995a). Generation particle beams of controlled dimensions and divergence: I. Theory of particle motion in aerodynamic lenses and nozzle expansions. *Aerosol Science and Technology*, *22*, 293–313.

Liu, P., Ziemann, P. J., Kittelson, D. B., & McMurry, P. H. (1995b). Generation particle beams of controlled dimensions and divergence: II. Experimental evaluation of particle motion in aerodynamic lenses and nozzle expansions. *Aerosol Science and Technology*, *22*, 314–324.

Mahadevan, R., Lee, D., Sakurai, H., & Zachariah, M. R. (2002). Measurement of condensed-phase reaction kinetics in the aerosol phase using single particle mass spectrometry. *Journal of Physical Chemistry A*, *106*, 11083–11092.

Murphy, W.K., & Sears, G.W. (1964). Production of Particulate Beams. *Journal of Applied Physics*, 35, 1986–1987.

Noble, C. A., & Prather, K. A. (2000). Real-time single particle mass spectrometry: A historical review of a quarter century of chemical analysis of aerosols. *Mass Spectrometry Reviews*, *19*, 248–274.

Park, K., Lee, D., Rai, A., Mckherjee, D., & Zachariah, M. R. (2005). Size-resolved kinetic measurements of aluminum nanoparticle oxidation with single particle mass spectrometry. *Journal of Physical Chemistry B*, *109*, 7290–7299.

Reents, W. D., & Ge, Z. (2000). Simultaneous elemental composition and size distribution of submicron particles in real time using laser atomizer/ionization mass spectrometry. *Aerosol Science and Technology*, *33*, 122–134.

Schreiner, J., Schild, U., Voigt, C., & Mauersberger, K. (1999). Focusing of aerosols into a particle beam at pressures from 10 to 150 torr. *Aerosol Science and Technology*, *31*(5), 373–382.

Slowik, J. G., Stainken, K., Davidovits, P., Williams, L. R., Jayne, J., Kolb, C. E. et al. (2004). Particle morphology and density characterization by combined mobility and aerodynamic diameter measurements. Part 2: Application to combustion generated soot particles as a function of fuel equivalence ratio. *Aerosol Science and Technology*, *28*(12), 1206–1222.

Su, Y. X., Sipin, M. F., Furutani, H., & Prather, K. A. (2004). Development and characterization of an aerosol time-of-flight mass spectrometer with increased detection efficiency. *Analytical Chemistry*, *76*(3), 712–719.

Venkataraman, C., & Raymond, J. (1998). Estimating the lung deposition of particulate polycyclic aromatic hydrocarbons associated with multimodal urban aerosols. *Inhalation Toxicology*, *10*(3), 183–204.

Wang, X., Gidwani, A., Girshick, S. L., & McMurry, P. H. (2005). Aerodynamic focusing of nanoparticles: II. Numerical simulation of particle motion through aerodynamic lenses. *Aerosol Science and Technology*, *39*, 624–636.

Wang, X., Kruis, F. E., & McMury, P. H. (2005). Aerodynamic focusing of nanoparticles: I. Guidelines for designing aerodynamic lenses for nanoparticles. *Aerosol Science and Technology*, *39*, 611–623.

Wang, X., & McMurry, P. H. (2006a). An experimental study of nanoparticle focusing with aerodynamic lenses. *International Journal of Mass Spectrometry*, *258*, 30–36.

Wang, X., & McMurry, P. H. (2006b). A design tool for aerodynamic lens systems. *Aerosol Science and Technology*, *40*, 320–334.

Zhang, X., Smith, K. A., Worsnop, D. R., Jimenez, J., Jayne, J. T., & Kolb, C. E. (2002). A numerical characterization of particle beam collimation by an aerodynamic lens-nozzle system: Part I. An individual lens or nozzle. *Aerosol Science and Technology*, *36*, 617–631.

Zhang, X., Smith, K. A., Worsnop, D. R., Jimenez, J. L., Jayne, J. T., Kolb, C. E. et al. (2004). Numerical characterization of particle beam collimation: Part II. Integrated aerodynamic-lens-nozzle system. *Aerosol Science and Technology*, *38*, 619–638.